Research Square

Preprints are preliminary reports that have not undergone peer review.
They should not be considered conclusive, used to inform clinical practice,
or referenced by the media as validated information.

Spatial Alignment of Parkinson's Disease-Related Quantitative MRI Alterations with Dopaminergic Topography

Norbert Brüggemann

norbert.brueggemann@uni-luebeck.de

University of Luebeck

Marta Pokotylo
Norman Griebner
Luzian Weske
Martin Göttlich
Jan Uter
Julia Henkel
Jannik Prasuhn

Article

Keywords:

Posted Date: October 18th, 2026

DOI: https://doi.org/10.21203/rs.3.rs-11124894/v1

License: This work is licensed under a Creative Commons Attribution 4.0 International License.
Read Full License

Additional Declarations: There is **NO** Competing Interest.

Abstract

Objective

Parkinson's disease (PD) is characterized by a degeneration of dopaminergic neurons not only in the nigrostriatal pathways, but also in subcortical and cortical structures. Given the widespread dopaminergic innervation, PD dopamine-related dysfunction may contribute to microstructural alterations beyond the primary site of pathology. Multiparametric mapping (MPM) enables quantification of tissue biophysical properties informing the brain's microstructure. We hypothesized that PD-related MPM alterations would show distinct spatial associations with pre- and postsynaptic dopaminergic markers.

Methods

31 patients with PD and 68 healthy controls underwent a 3T MRI. We used unthresholded MPM t-maps derived from group-difference analysis to assess spatial correlation with PET-derived maps of the dopamine transporter (DAT), [^{18}F]-fluoro-L-DOPA (FDOPA), and dopamine D1 and D2 receptors.

Results

Proton density alterations negatively correlated with DAT (rho = 0.355, $p_{spatial}$ = 0.0010) and FDOPA (rho = 0.168, p_{FDR} = 0.0080) across whole-brain gray matter. Subcortically, MPM-dopaminergic associations were structure-specific, showing concordant, same-direction associations between FDOPA and D1. Cortically, associations were more consistent, predominantly negative and driven by DAT and FDOPA. Within cortical ROIs, presupplementary and supplementary motor areas showed the most robust associations, driven by proton density (preSMA: rho = 0.428 to 0.760; SMA: rho = 0.284 to 0.789, all p_{FDR} < 0.0001).

Interpretation:

PD-related microstructural-dopaminergic associations were structure- and modality-specific. Subcortically, FDOPA and D1 consistently tracked microstructural alterations, potentially reflecting coupled degeneration of dopaminergic synthesis capacity and postsynaptic receptor density. Cortically, DAT and FDOPA most robustly tracked proton density-related alterations, potentially indicating distinct and mainly neuroinflammation-driven microstructural processes beyond the primary nigrostriatal network.

Introduction

Parkinson's disease (PD) is a progressive neurodegenerative disorder characterized by irreversible neuronal loss, primarily originating in the substantia nigra pars compacta (SNc)[1]. Dopaminergic neurons are the primary population affected in PD due to their structural vulnerability, including highly branched, long axons, and metabolic vulnerability resulting from the toxic profile of dopamine synthesis[2]. PD is primarily characterized by motor symptoms attributable to neurodegeneration of subcortical nuclei, such as the basal ganglia, which are innervated by dopaminergic projections from the SN[3,4]. However, dopaminergic innervation extends to the neocortex through mesocortical and other midbrain dopaminergic pathways[5,6], raising the possibility that disease-related neurodegeneration is not confined to the primary site of pathology, but instead follows the broader pattern of dopaminergic architecture.

Quantitative magnetic resonance imaging (MRI) techniques such as multiparametric mapping (MPM) can be used to investigate the biophysical properties of the tissue, including the effective transverse relaxation rate (R2*), a biomarker of paramagnetic substances such as iron, allowing an *in vivo* spatial assessment of iron content in the brain[8,9]. Additionally, MPM quantifies the longitudinal relaxation rate (R1) and magnetic transfer saturation (MTsat), which serve as *in vivo* biomarkers of macromolecular and myelin content, as well as proton density, which reflects free-water content, enabling investigation of demyelination/remyelination, neuroinflammation processes, and neuronal integrity[10–12]. MPM provides a meaningful way to assess PD-related microstructural changes of the brain, but it cannot establish whether these changes are organized around dopaminergic architecture.

For direct assessment, PD-related spatial alterations in MPM can be related to normative maps of dopaminergic architecture, using (PET)-derived maps of dopaminergic neurotransmission in the human brain[13]. The available PET-derived spatial maps of dopamine transporter (DAT), [^{18}F]-fluoro-L-DOPA (FDOPA), and dopamine receptors D1 and D2 (D1 and D2) provide an additional layer to the biological characterization of pre- (FDOPA and DAT) and post-synaptic (D1 and D2) dopaminergic functions in the brain. By spatially correlating MPM-derived differences between patients with PD (PwPD) and healthy controls (HCs) with normative dopaminergic maps, we can investigate whether the topography of the MPM alterations in PD follows the topography of underlying dopaminergic architecture.

Given differences in baseline dopaminergic innervation between subcortical and cortical regions, we hypothesized that the MPM-dopaminergic relationship would be region-specific rather than uniform across the brain[14]. Additionally, we expected a differential pattern of association between D1 and D2, given their functional specialization and differential expression[14]. To investigate this, we used the PD-specific HybraPD atlas[15] of subcortical regions and the Human Motor Area Template (HMAT)[16] of cortical regions to assess regional MPM-dopaminergic associations.

Results

Demographic and clinical assessment. We included 68 HCs and 31 PwPD, with comparable age ($p = 0.720$) and sex distribution ($p = 1.000$). Our PwPD cohort comprised moderately affected patients with

an average Movement Disorder Society Unified Parkinson's Disease Rating Scale subscore III (MDS-UPDRS-III) score of 28.6 ± 15.5 and a disease duration of 4.5 ± 4.3 years. As patients were assessed in the ON state, the average levodopa equivalent daily dose (LEDD) was 512.6 ± 365.6 (Table 1).

Table 1
Demographic and clinical characteristics.

number	**PwPD**	**HCs**	**p-value**
	31	**68**	
male/female	13/18	28/40	1.000 [1]
age (years)	64.9 ± 9.3	65.6 ± 8.1	0.720 [2]
MDS-UPDRS-III	28.6 ± 15.5	n.a.	
LEDD	512.6 ± 365.6	n.a.	
Disease duration (years)	4.5 ± 4.3	n.a.	
Hoehn and Yahr stage	2 [1–2]	n.a.	

Mean values and standard deviations are quoted. Values in square brackets represent the interquartile range. [1] according to a χ^2-test; [2] two-sample t-test applied. HCs: healthy controls. LEDD: levodopa equivalent daily dose. MoCA: Montreal Cognitive Assessment. MDS-UPDRS-III: Movement Disorders Society's Unified Parkinson's Disease Rating Scale (subscore III). n.a.: not available. PwPD: patients with Parkinson's disease.

Whole-brain gray matter MPM alterations correlated with presynaptic dopaminergic markers only. In the whole-brain gray matter, we observed significant associations between MPM modalities and presynaptic dopaminergic markers only (DAT and FDOPA, Fig. 1). Proton density negatively correlated with DAT (rho = -0.355, $p_{spatial}$ = 0.0010) and FDOPA (rho = -0.168, p_{FDR} = 0.0080), while R2* positively correlated with FDOPA (rho = 0.126, p_{FDR} = 0.0100) and MTsat with DAT (rho = 0.168, p_{FDR} = 0.0310).

R1 and proton density were negatively associated with FDOPA and D1, tracking microstructural changes in the basal ganglia. Within the basal ganglia system, proton density showed the most prominent associations with dopaminergic markers in the globus pallidus (GP). FDOPA and D1 negatively correlated with proton density in the GP (rho = -0.297 and − 0.336; p_{FDR} < 0.0300) and the GP external segment (GPe, rho = -0.295 and − 0.309; p_{FDR} < 0.0473). The putamen was characterized by negative R1-FDOPA and R1-D1 associations (rho = -0.439 and − 0.352, p_{FDR} < 0.0456, Fig. 2, Table S1). Within the substantia nigra, we observed associations that survived the spatial autocorrelation test but not the FDR correction: positive R2*-FDOPA (rho = 0.523, $p_{spatial}$ = 0.0399, p_{FDR} = 0.1853) and R2*-D1 (rho = 0.528, $p_{spatial}$ = 0.0353, p_{FDR} = 0.1791) associations. Caudate nucleus (CN) yielded a single positive MTsat-FDOPA association (rho = 0.249, p_{FDR} = 0.0425).

Across the nigrostriatal system, MTsat yielded the most robust positive correlations with FDOPA, D1, and D2 in ventral pallidum (VeP, rho = 0.428 to 0.567, $p_{FDR} < 0.0425$). Additionally, MTsat positively correlated with FDOPA and D1 in the nucleus accumbens (NAC, rho = 0.476 and 0.573; $p_{FDR} < 0.0308$) and red nucleus (RN, rho = 0.507 and 0.633; $p_{FDR} < 0.0001$).

preSMA and SMA showed the most robust MPM-dopaminergic marker associations, primarily driven by proton density. Presupplementary motor area (preSMA) and supplementary motor area (SMA) demonstrated the most robust associations with dopaminergic markers, characterized by negative associations with dopaminergic markers across all four MPM modalities, primarily driven by proton density (preSMA: rho = -0.428 to -0.760, SMA: rho = -0.284 to -0.789, all $p_{FDR} < 0.0001$). PMd presented a similar pattern, restricted to negative associations between R1, R2*, MTsat, and all dopaminergic features (rho = -0.098 to -0.460, $p_{FDR} < 0.0001$). We observed a similar but weaker pattern in the primary motor area (M1, rho = -0.044 to -0.265, $p_{FDR} < 0.0325$). Within the primary somatosensory area (S1), associations were restricted to negative R1 and DAT, FDOPA, and D1 correlations (rho = -0.115 to -0.187, $p_{FDR} < 0.0404$). Meanwhile, D2 positively, but weakly correlated with R2* (rho = 0.115, $p_{FDR} = 0.0269$), proton density (rho = 0.080, $p_{FDR} = 0.0082$), and MTsat (rho = 0.073, $p_{FDR} < 0.0001$) in S1.

Subcortical and cortical ROIs showed distinct MPM-dopaminergic association patterns.

Among identified associations, we observed differential patterns among subcortical and cortical ROIs. Subcortical ROIs showed concordant, same-direction associations with FDOPA and D1 (Fig. 2), including negative associations in GP and GPe and positive associations in VeP, NAC, and RN. In contrast, cortical ROIs showed negative associations, primarily driven by DAT and FDOPA, including in the preSMA, SMA, and PMd. This divergence suggests that subcortical MPM-dopaminergic associations occurred in a modality- and structure-specific manner, with FDOPA and D1 tracking together across most ROIs, while cortical associations uniformly tracked presynaptic markers.

Discussion

In this study, we investigated the spatial association between PD-related MPM alterations and normative PET-derived maps of DAT, FDOPA, D1, and D2 to examine the relationship between microstructural changes and baseline dopaminergic neurotransmission architecture. We observed a divergent spatial pattern characterized by positive, concordant MPM associations with FDOPA and D1 in subcortical ROIs and inverse associations, predominantly with presynaptic markers, in cortical ROIs. These findings suggest that PD-related MPM alterations are not uniformly related to underlying dopaminergic architecture and instead show region- and modality-specific relationships.

Proton density consistently negatively correlated with presynaptic dopaminergic markers, showing the strongest associations with the preSMA and SMA (rho = -0.760 and − 0.789, respectively). These findings indicate that regions with higher proton density tend to correspond to regions with lower normative presynaptic dopaminergic markers in PwPD. Elevated free water has been associated with

inflammatory processes, suggesting that neuroinflammatory-related MPM changes may be spatially organized around regions with sparse dopaminergic innervation. However, because proton density is a non-specific marker of free water, this interpretation is hypothesis-generating and requires further validation. These inverse MPM-dopaminergic associations may potentially reflect secondary or network-level consequences of basal ganglia dysfunction rather than primary degeneration in these regions, including altered cortico-basal ganglia-thalamocortical signaling[25–27].

In subcortical regions, FDOPA and D1 density concordantly associated with subcortical MPM alterations, while DAT and FDOPA density concordantly associated with cortical MPM alterations. This divergence can be partially explained by the biological roles of the dopaminergic markers assessed. FDOPA is considered a marker of dopamine synthesis as it probes aromatic L-amino acid decarboxylase (AADC) activity[28], which can be relatively preserved or even be upregulated in early- and moderate-stage PwPD as a compensatory response to terminal loss[29], while DAT probes presynaptic terminal density by reuptake-site availability[30]. D1 receptors are expressed on striatonigral projection neurons of the basal ganglia “direct pathway”, which are anatomically coupled to presynaptic dopaminergic input in the striatum and pallidum[31]. Therefore, the identified subcortical MPM alterations tracking FDOPA and D1 topography are consistent with pathology being distributed across the full, coupled presynaptic synthesis-postsynaptic receptor unit, rather than a single component. Because D1 and D2 are expressed on relatively resilient dendrites and soma, rather than vulnerable presynaptic terminals[33], a global lack of MPM-D1 and -D2 associations further reinforced the idea that cortical microstructural alterations may primarily relate to presynaptic tomography, with the postsynaptic receptor system becoming implicated in later disease stages[34]. Importantly, small subcortical ROIs such as SN are particularly susceptible to partial-volume effects and spatial blurring, limiting the anatomical precision of our region-specific findings. Therefore, the biological interpretation should be considered provisional, which requires further validation with higher-resolution acquisition or smaller smoothing kernels.

The region-specific associations suggest that distinct biological processes may align differently with dopaminergic architecture. For instance, R2* positively associated with dopaminergic markers in SN (although not FDR-significant), potentially relating to iron-related changes implicated in nigral cell loss[35]. Additionally, MTsat was positively associated with dopaminergic markers in the ventral striatum and midbrain structures dense in presynaptic terminals[36], potentially reflecting myelin-related changes. Proton density yielded inverse associations extending into the pallidum and cortex, which lie further along dopaminergic projections. Collectively, these findings suggest that PD-related microstructural alterations may reflect multiple, partially independent biological processes that may preferentially align with coupled presynaptic-postsynaptic units or spatially dissociate from the dopaminergic presynaptic architecture.

Several limitations should be considered. First, our cross-sectional design limits our ability to causally interpret spatial associations, and longitudinal data are needed to establish the dynamic nature of microstructural-dopaminergic associations. Second, because our cohort comprised early- to moderate-

stage PwPD, the identified associations may not generalize to advanced-stage PD. Third, our relatively modest sample size may have prevented us from identifying smaller-magnitude or more spatially localized associations, especially in smaller ROIs. Therefore, future work needs larger, more heterogeneous PwPD cohorts.

We intentionally used a normative dataset to assess whether PD-related microstructural alterations preferentially occur in regions that are at baseline dopamine-rich or dopamine-poor. Subsequent research may build on our findings by using complementary approaches, including PET imaging, to assess patient-specific dopaminergic architecture and relate it to microstructural alterations, as dopaminergic architecture is known to vary substantially across PwPD[37]. However, such approach may be greatly confounded by dopaminergic medication, as levodopa administration is known to alter dopaminergic functionality independently of disease-related effects[38,39], with no effect on brain's micro- and macrostructure[40–42]. Because we lack meaningful approaches to disentangle disease-driven from medication-driven effects on PET markers, this remains a challenge and would need to be addressed in medication-OFF state or medication-naive cohorts, which in turn are limited to early- to moderate-stage PwPD, since most advanced-stage PwPD would require ongoing dopaminergic treatment.

In conclusion, our findings indicate that PD-related microstructural alterations may be spatially coupled to baseline dopaminergic architecture in the basal ganglia and inversely associated with it in cortical regions. Proton density was consistently negatively associated with presynaptic dopaminergic markers, while R2* and MTsat showed positive, region-specific associations with dopaminergic markers in nigrostriatal structures. Therefore, MPM modalities may be differentially sensitive to distinct parts of PD pathology that differentially co-localize with baseline dopaminergic architecture across the brain. Future research should adopt a longitudinal design with a group-level PET dataset and integration of additional data to assess the temporal and causal relationship in detail.

Methods

Experimental design and participants

We recruited participants from our inpatient and outpatient clinics in the Department of Neurology at University Hospital Schleswig-Holstein (Campus Luebeck). Parkinson's disease was diagnosed as clinically established PD according to the Movement Disorder Society Clinical Diagnostic Criteria, representing the highest level of diagnostic certainty attainable on clinical grounds within this framework[17]. Our inclusion criteria comprised an age between 50 and 80 years and no concomitant neurological/psychiatric conditions. Exclusion criteria included comorbidities affecting the ability to provide written consent, MRI contraindications, diagnosis of atypical or secondary Parkinsonism, history of alcohol abuse, or history or presence of structural brain diseases. Every participant provided written informed consent. Every participant underwent a clinical examination and one MRI session. PwPD were examined and imaged in the medication ON stage. The MRI dataset from this cohort has been previously

reported[18,19], and this work reports a novel secondary analysis. The study adhered to the Declaration of Helsinki and was approved by the local ethics committee at the University of Luebeck, Germany (AZ: 2024 – 302_2). Prior to study inclusion, every participant provided written informed consent.

Image acquisition and voxel-based quantification

MRI was performed at the Center for Brain, Behavior, and Metabolism Core Facility at the University of Luebeck, using a 3 Tesla Siemens Magnetom Skyra scanner with a 64-channel head/neck coil. Using a multi-echo 3D fast low-angle shot (FLASH) sequence, we acquired T1-, proton density-, and magnetization transfer-weighted images, as previously described[10]. All acquisitions were acquired in 3D with 240 contiguous slices, 1.0 mm isotropic resolution, a field of view of 256 × 176 mm² (phase FoV 68.8%), GRAPPA acceleration factor 2, and partial Fourier 6/8 in the slice direction. The receiver bandwidth for all echoes was 440 Hz/px. Inline distortion correction (2D mode) and prescan normalization were enabled. The combination of T1-weighted acquisition (TR = 19.0 ms, flip angle = 20°, six echoes with TE = 2.20/4.70/7.20/9.70/12.20/15.00 ms, 8 minutes); the proton density-weighted acquisition (TR = 24.0 ms, flip angle = 20°, eight echoes with TE = 2.20/4.70/7.20/9.70/12.20/15.00/17.50/20.00 ms, 11 minutes) and the magnetic transfer-weighted acquisition (TR = 37.0 ms, flip angle = 20°, six echoes with TE = 2.20/4.70/7.20/9.70/12.20/15.00 ms, 7 minutes), resulted in a total acquisition time of 26 minutes. A neuroradiologist reviewed all datasets to exclude concurrent conditions and to assess visual artifacts (e.g., extensive head motion). We also quantitatively evaluated the data quality using voxel-wise z-scores. Our exclusion criteria included participants with severe visible motion artifacts (ringing and blurring) and excessive quantitative measures, defined as z-scores greater than 2 standard deviations above the mean.

We processed the acquired images using the hMRI toolbox[20] implemented in SPM25 (Statistical Parametric Mapping 25)[21] and MATLAB (R2024b, The MathWorks Inc., Natick, MA, USA). We reconfigured the hMRI toolbox with scanner-specific settings using a custom-written MATLAB script. Acquired T1-, proton density-, and magnetic transfer-weighted images served as input. We generated MPM maps after B_1 correction using the UNICORT algorithm and after radiofrequency receive-sensitivity bias correction using unified segmentation. We preprocessed the MPM maps using the hMRI toolbox pipeline, including segmentation (into gray matter, white matter, and cerebrospinal fluid tissue maps), nonlinear spatial registration to MNI space, and tissue-weighted smoothing[22–24]. Our preprocessing settings included resampling to a voxel size of 1 × 1 × 1 mm^3, and spatial Gaussian smoothing with a 6 × 6 × 6 mm FWHM kernel.

Statistical analysis: multiparametric mapping group differences analysis

We performed the group-level analysis in SPM25 within MATLAB. Using a two-sample t-test and controlling for age and sex, we derived t-maps of PD-related differences across all four MPM modalities (R2*, R1, proton density, and MTsat). We assessed only one contrast, generating t-maps showing higher MPM-derived values in PwPD than in HCs (PwPD > HCs). All t-maps were generated using explicit masks, including the tissue probability mask for gray matter incorporated into the SPM25 environment, and masks derived from the HybraPD atlas[15] and the HMAT[16], thereby assessing group differences within specific regions of interest (ROIs). Statistically significant group differences from this analysis were previously reported elsewhere and were mainly located within cortical regions[18,19]. Overall, we assessed group differences across 27 ROIs, including whole-brain gray matter, 20 subcortical regions, and 6 motor cortical regions. For all bilateral structures, we combined left- and right-hemisphere ROI masks before analysis. We generated four t-maps for each ROI, corresponding to PwPD > HCs R2*, R1, proton density, and MTsat values.

Statistical analysis: spatial correlation between PD-related microstructure and neurotransmitter receptor maps

Using the original unthresholded MPM-derived t-maps and PET-derived dopaminergic neurotransmission maps, we performed voxel-wise spatial correlation in R (v4.5.3; R Code Team, 2026; R Foundation for Statistical Computing, Vienna, Austria) using oro.nifti package (v0.11.4), dplyr (v1.2.1) packages, and modified.ttest function from the SpatialPack package (v0.4.1). We obtained PET-derived maps of DAT, FDOPA, D1, and D2 from a previously published study[13]. We performed 16 correlation tests per ROI (four t-maps: R2*, R1, proton density, MTsat, and four dopaminergic maps: DAT, FDOPA, D1, D2). We restricted the analyses to voxels containing valid PwPD > HCs t-values and valid neurotransmitter receptor map values. For each analysis, we calculated Spearman's correlation coefficient (rho) and 95% confidence intervals.

To control for spatial autocorrelation, we used Dutilleul's modified t-test, which estimates the spatial autocorrelation of the MPM t-map and dopaminergic marker map from their voxel-wise covariance and derives a corrected effective sample size (ESS). We calculated 95% confidence intervals using ESS. To control for multiple comparisons, we implemented the Benjamini-Hochberg false discovery rate (FDR) procedure using Dutilleul's modified t-test-derived p-values ($p_{spatial}$) across all ROI × dopaminergic marker × MPM modality, yielding p_{FDR}. We report p_{FDR} as the primary significance metric throughout the Results section. Tables S1 and S2 provide detailed statistics. Visual presentations were generated in R (v4.5.3) using the ggplot2 (v4.0.2) and patchwork (v1.3.2) packages within RStudio (v2026.01.1 + 403; Posit Software, PBC, Boston, MA, USA).

Declarations

Conflicts of interest

Nothing to report.

Authors contribution

Conceptualization: M.M.P., J.P.; Formal analysis: M.M.P., L.W.; Investigation: N.G., J.U., J.H.; Writing – Original Draft: M.M.P.; Writing – Editing & Review: M.G., N.B., J.P.; Visualization: M.M.P., Supervision: J.P.; Project Administration: J.P.; Funding Acquisition: N.B.

Acknowledgments

This work was supported by funding provided by the Deutsche Forschungsgemeinschaft (DFG; Research Unit FOR2488, N.B.), and by the JPND Consortium Control-PD (N.B.). The author JP gratefully acknowledges support from the Detlef Zillikens Clinician Scientist Academy of Precision Health in Schleswig-Holstein (PHSH), the Clinician Scientist Academy Lübeck, the Michael J. Fox Foundation for Parkinson's Research (MJFF-025746, -028069, and – 028070, and), and the Else Kröner-Fresenius-Stiftung (2023_EKEA. 168).

Data availability

The data that support the findings of this study are available from the corresponding author upon reasonable request.

References

1. Bloem BR, Okun MS, Klein C. Parkinson's disease. *The Lancet*. 2021;397(10291):2284–2303. doi:10.1016/S0140-6736(21)00218-X
2. Chan CS, Gertler TS, Surmeier DJ. A molecular basis for the increased vulnerability of substantia nigra dopamine neurons in aging and Parkinson's disease. *Mov Disord*. 2010;25(S1). doi:10.1002/mds.22801
3. Gcwensa NZ, Russell DL, Cowell RM, Volpicelli-Daley LA. Molecular Mechanisms Underlying Synaptic and Axon Degeneration in Parkinson's Disease. *Front Cell Neurosci*. 2021;15:626128. doi:10.3389/fncel.2021.626128
4. Kordower JH, Olanow CW, Dodiya HB, et al. Disease duration and the integrity of the nigrostriatal system in Parkinson's disease. *Brain*. 2013;136(8):2419–2431. doi:10.1093/brain/awt192
5. Hosp JA, Coenen VA, Rijntjes M, et al. Ventral tegmental area connections to motor and sensory cortical fields in humans. *Brain Struct Funct*. 2019;224(8):2839–2855. doi:10.1007/s00429-019-01939-0

6. Hosp JA, Pekanovic A, Rioult-Pedotti MS, Luft AR. Dopaminergic Projections from Midbrain to Primary Motor Cortex Mediate Motor Skill Learning. *J Neurosci*. 2011;31(7):2481–2487. doi:10.1523/JNEUROSCI.5411-10.2011
7. Brammerloh M, Morawski M, Friedrich I, et al. Measuring the iron content of dopaminergic neurons in substantia nigra with MRI relaxometry. *NeuroImage*. 2021;239:118255. doi:10.1016/j.neuroimage.2021.118255
8. Draganski B, Ashburner J, Hutton C, et al. Regional specificity of MRI contrast parameter changes in normal ageing revealed by voxel-based quantification (VBQ). *NeuroImage*. 2011;55(4):1423–1434. doi:10.1016/j.neuroimage.2011.01.052
9. Stüber C, Morawski M, Schäfer A, et al. Myelin and iron concentration in the human brain: A quantitative study of MRI contrast. *NeuroImage*. 2014;93:95–106. doi:10.1016/j.neuroimage.2014.02.026
10. Weiskopf N, Suckling J, Williams G, et al. Quantitative multi-parameter mapping of R1, PD*, MT, and R2* at 3T: a multi-center validation. *Front Neurosci*. 2013;7. doi:10.3389/fnins.2013.00095
11. Lorio S, Tierney TM, McDowell A, et al. Flexible proton density (PD) mapping using multi-contrast variable flip angle (VFA) data. *NeuroImage*. 2019;186:464–475. doi:10.1016/j.neuroimage.2018.11.023
12. Callaghan MF, Helms G, Lutti A, Mohammadi S, Weiskopf N. A general linear relaxometry model of R_1 using imaging data: General Linear Relaxometry Model of R1. *Magn Reson Med*. 2015;73(3):1309–1314. doi:10.1002/mrm.25210
13. Hansen JY, Shafiei G, Markello RD, et al. Mapping neurotransmitter systems to the structural and functional organization of the human neocortex. *Nat Neurosci*. 2022;25(11):1569–1581. doi:10.1038/s41593-022-01186-3
14. Keyser JD. Subtypes and localization of dopamine receptors in human brain. *Neurochem Int*. 1993;22(2):83–93. doi:10.1016/0197-0186(93)90001-L
15. Yu B, Li L, Guan X, et al. HybraPD atlas: Towards precise subcortical nuclei segmentation using multimodality medical images in patients with Parkinson disease. *Hum Brain Mapp*. 2021;42(13):4399–4421. doi:10.1002/hbm.25556
16. Mayka MA, Corcos DM, Leurgans SE, Vaillancourt DE. Three-dimensional locations and boundaries of motor and premotor cortices as defined by functional brain imaging: A meta-analysis. *NeuroImage*. 2006;31(4):1453–1474. doi:10.1016/j.neuroimage.2006.02.004
17. Postuma RB, Berg D, Stern M, et al. MDS clinical diagnostic criteria for Parkinson's disease: MDS-PD Clinical Diagnostic Criteria. *Mov Disord*. 2015;30(12):1591–1601. doi:10.1002/mds.26424
18. Pokotylo MM, Göttlich M, Schmidt L, et al. In-vivo histology of Parkinson's disease using quantitative multiparametric mapping. *Npj Park Dis*. 2026;12(1):82. doi:10.1038/s41531-026-01329-4
19. Pokotylo MM, Göttlich M, Schmidt L, et al. Spatial Coupling between Parkinson's Disease-Related Quantitative MRI Alterations and Mitochondrial Brain Architecture. *In Review*. Preprint posted online May 20, 2026. doi:10.21203/rs.3.rs-9643832/v1

20. Tabelow K, Balteau E, Ashburner J, et al. hMRI – A toolbox for quantitative MRI in neuroscience and clinical research. *NeuroImage*. 2019;194:191–210. doi:10.1016/j.neuroimage.2019.01.029
21. Tierney TM, Alexander NA, Ashburner J, et al. SPM 25: open source neuroimaging analysis software. *J Open Source Softw*. 2025;10(110):8103. doi:10.21105/joss.08103
22. Draganski B, Ashburner J, Hutton C, et al. Regional specificity of MRI contrast parameter changes in normal ageing revealed by voxel-based quantification (VBQ). *NeuroImage*. 2011;55(4):1423–1434. doi:10.1016/j.neuroimage.2011.01.052
23. Ashburner J. A fast diffeomorphic image registration algorithm. *NeuroImage*. 2007;38(1):95–113. doi:10.1016/j.neuroimage.2007.07.007
24. Ashburner J, Friston KJ. Unified segmentation. *NeuroImage*. 2005;26(3):839–851. doi:10.1016/j.neuroimage.2005.02.018
25. Albin RL, Young AB, Penney JB. The functional anatomy of basal ganglia disorders. *Trends Neurosci*. 1989;12(10):366–375. doi:10.1016/0166-2236(89)90074-X
26. Wei L, Zhang J, Long Z, et al. Reduced topological efficiency in cortical-basal Ganglia motor network of Parkinson's disease: a resting state fMRI study. *PloS One*. 2014;9(10):e108124. doi:10.1371/journal.pone.0108124
27. Casarotto S, Turco F, Comanducci A, et al. Excitability of the supplementary motor area in Parkinson's disease depends on subcortical damage. *Brain Stimulat*. 2019;12(1):152–160. doi:10.1016/j.brs.2018.10.011
28. Biju G, De La Fuente-Fernández R. Dopaminergic function and progression of Parkinson's disease: PET findings. *Parkinsonism Relat Disord*. 2009;15:S38-S40. doi:10.1016/S1353-8020(09)70833-8
29. Lee CS, Samii A, Sossi V, et al. In vivo positron emission tomographic evidence for compensatory changes in presynaptic dopaminergic nerve terminals in Parkinson's disease. *Ann Neurol*. 2000;47(4):493–503. doi:10.1002/1531-8249(200004)47:4%3C493::AID-ANA13%3E3.0.CO;2-4
30. Brooks DJ. Imaging Dopamine Transporters in Parkinson's Disease. *Biomark Med*. 2010;4(5):651–660. doi:10.2217/bmm.10.86
31. Gerfen CR, Engber TM, Mahan LC, et al. D_1 and D_2 Dopamine Receptor-regulated Gene Expression of Striatonigral and Striatopallidal Neurons. *Science*. 1990;250(4986):1429–1432. doi:10.1126/science.2147780
32. Islam KUS, Meli N, Blaess S. The Development of the Mesoprefrontal Dopaminergic System in Health and Disease. *Front Neural Circuits*. 2021;15:746582. doi:10.3389/fncir.2021.746582
33. Wong YC, Luk K, Purtell K, et al. Neuronal vulnerability in Parkinson disease: Should the focus be on axons and synaptic terminals? *Mov Disord*. 2019;34(10):1406–1422. doi:10.1002/mds.27823
34. Kaasinen V, Vahlberg T, Stoessl AJ, Strafella AP, Antonini A. Dopamine Receptors in Parkinson's Disease: A Meta-Analysis of Imaging Studies. *Mov Disord*. 2021;36(8):1781–1791. doi:10.1002/mds.28632

35. Depierreux F, Parmentier E, Mackels L, et al. Parkinson's disease multimodal imaging: F-DOPA PET, neuromelanin-sensitive and quantitative iron-sensitive MRI. *Npj Park Dis*. 2021;7(1):57. doi:10.1038/s41531-021-00199-2
36. Threlfell S, Cragg SJ. Dopamine Signaling in Dorsal Versus Ventral Striatum: The Dynamic Role of Cholinergic Interneurons. *Front Syst Neurosci*. 2011;5. doi:10.3389/fnsys.2011.00011
37. Suh M, Im JH, Choi H, Kim H, Cheon GJ, Jeon B. Unsupervised clustering of dopamine transporter PET imaging discovers heterogeneity of parkinsonism. *Hum Brain Mapp*. 2020;41(16):4744–4752. doi:10.1002/hbm.25155
38. Tedroff J, Pedersen M, Aquilonius SM, Hartvig P, Jacobsson G, Långström B. Levodopa-induced changes in synaptic dopamine in patients with Parkinson's disease as measured by [^{11} C]raclopride displacement and PET. *Neurology*. 1996;46(5):1430–1430. doi:10.1212/WNL.46.5.1430
39. Politis M, Wilson H, Wu K, Brooks DJ, Piccini P. Chronic exposure to dopamine agonists affects the integrity of striatal D2 receptors in Parkinson's patients. *NeuroImage Clin*. 2017;16:455–460. doi:10.1016/j.nicl.2017.08.013
40. Fahn S, Oakes D, Shoulson I, et al. Levodopa and the progression of Parkinson's disease. *N Engl J Med*. 2004;351(24):2498–2508. doi:10.1056/NEJMoa033447
41. Frequin HL, Verschuur CVM, Suwijn SR, et al. Long-Term Follow-Up of the LEAP Study: Early Versus Delayed Levodopa in Early Parkinson's Disease. *Mov Disord*. 2024;39(6):975–982. doi:10.1002/mds.29796
42. Verschuur CVM, Suwijn SR, Boel JA, et al. Randomized Delayed-Start Trial of Levodopa in Parkinson's Disease. *N Engl J Med*. 2019;380(4):315–324. doi:10.1056/NEJMoa1809983

Figures

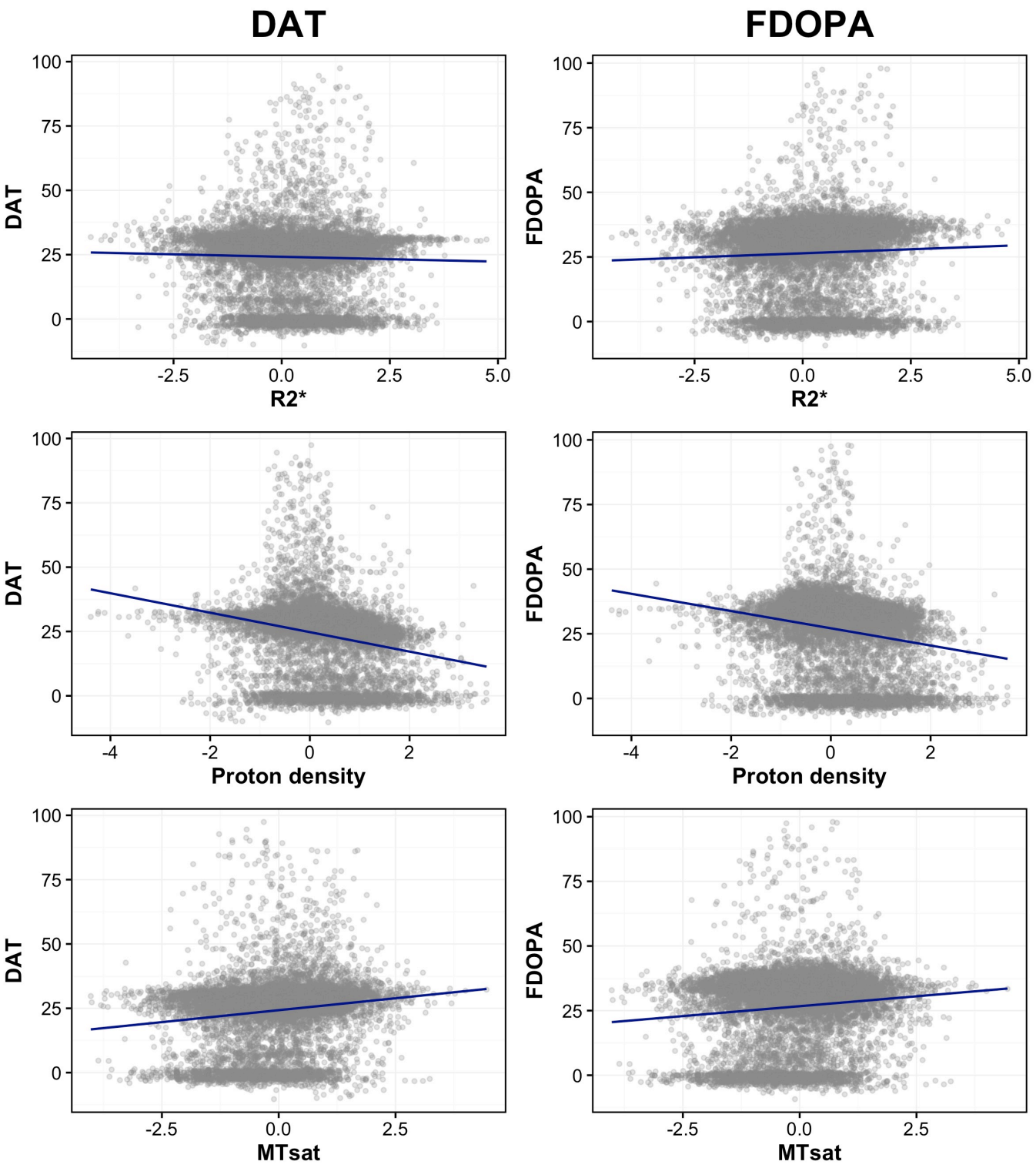


Figure 1

Spatial associations between PwPD-derived MPM measures and DAT and FDOPA in the whole-brain GM. Representative scatter plots illustrate the spatial relationships between MPM-derived t-values (rows: R2*, proton density, MTsat) and PET-derived dopamine marker t-values (columns: DAT, FDOPA) across the whole-brain GM. DAT: dopamine transporter. FDOPA: [^{18}F]-fluoro-L-DOPA. GM: gray matter.

MPM: multiparametric mapping. MTsat: magnetic transfer saturation. PET: positron emission tomography. PwPD: patients with Parkinson's disease. R2*: effective transverse relaxation rate.

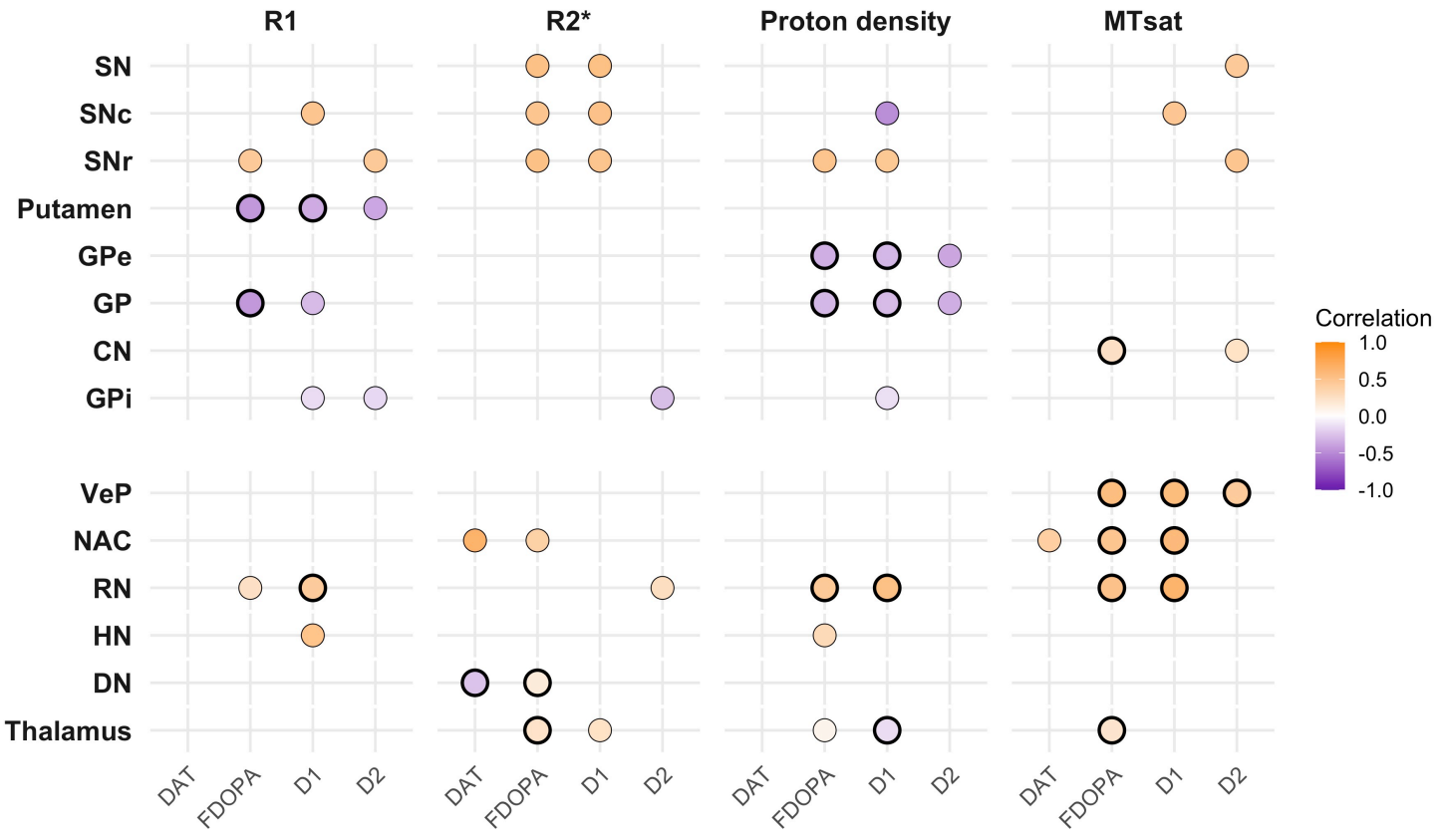


Figure 2

Regional association between PwPD-derived MPM measures and PET-derived dopaminergic measures within the subcortical HybraPD-derived ROIs. Comparison plot demonstrating spatial correlation between MPM-derived measures and PET-derived dopaminergic markers. Regions are ordered from bottom to top by association strength across all dopaminergic markers and MPM measures. Empty cells indicate associations that did not reach significance ($p < 0.05$) using Dutilleul's modified t-test correcting for spatial autocorrelation. Bold-bordered cells indicate associations that additionally survived false-discovery rate correction. CN: caudate nucleus. D1: dopamine D1 receptor. D2: dopamine D2 receptor. DAT: dopamine transporter. DN: dentate nucleus. FDOPA: [^{18}F]-fluoro-L-DOPA. GP: globus pallidus. GPe/GPi: globus pallidus external/internal segment. HN: habenular nucleus. MPM: multiparametric mapping. MTsat: magnetization transfer saturation. NAC: nucleus accumbens. PET: positron emission tomography. PwPD: patients with Parkinson's disease. R1: longitudinal relaxation rate. R2*: effective transverse relaxation rate. RN: red nucleus. ROIs: region of interest. SN: substantia nigra. SNc/SNr: substantia nigra pars compacta/reticulata. VeP: ventral pallidum.

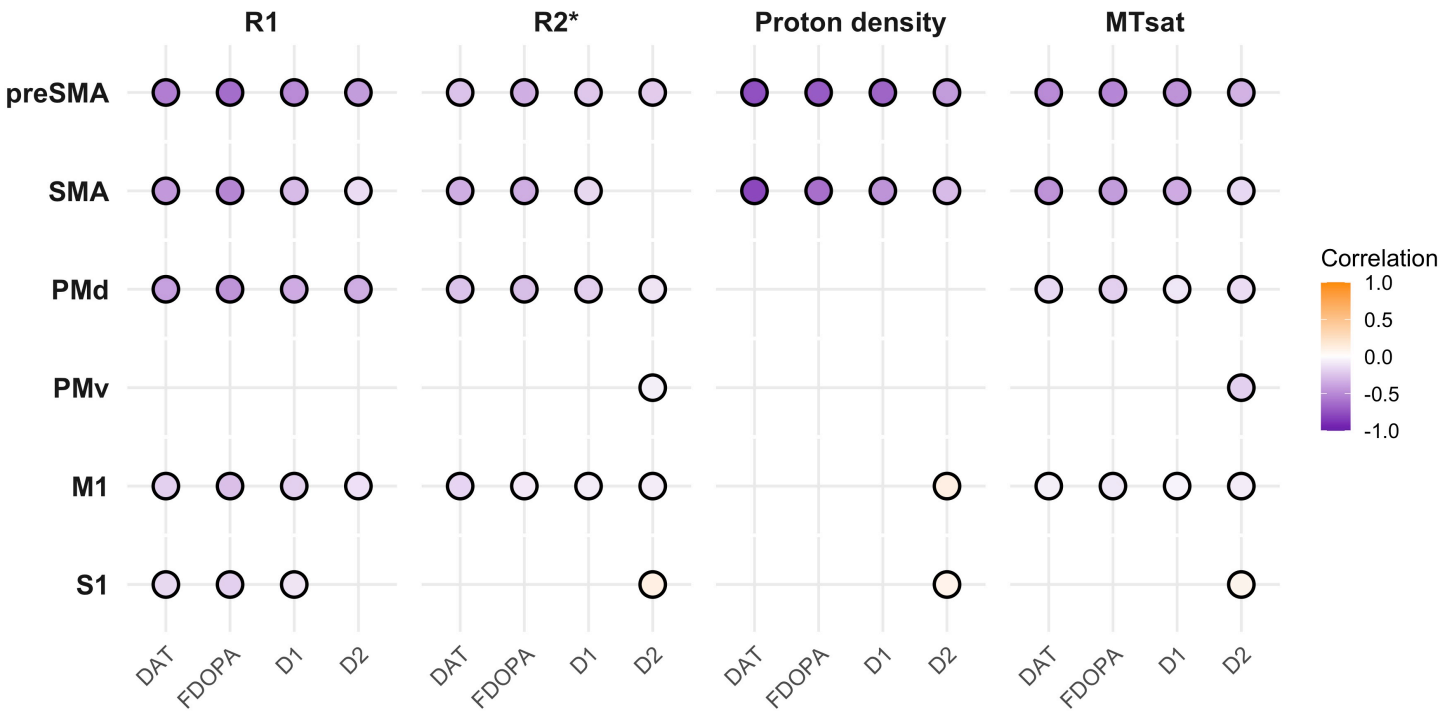


Figure 3

Regional association between PwPD-derived MPM measures and PET-derived dopaminergic measures within the cortical HMAT-derived ROIs. Comparison plot demonstrating spatial correlation between MPM-derived measures and PET-derived dopaminergic markers. Regions are ordered from bottom to top by association strength across all dopaminergic markers and MPM measures. Empty cells indicate associations that did not reach significance ($p < 0.05$) using Dutilleul's modified t-test correcting for spatial autocorrelation. Bold-bordered cells indicate associations that additionally survived false-discovery rate correction. D1: dopamine D1 receptor D2: dopamine D2 receptor. DAT: dopamine transporter. FDOPA: [^{18}F]-fluoro-L-DOPA. HMAT: human motor area template. M1: primary motor area. MPM: multiparametric mapping. MTsat: magnetization transfer saturation. PET: positron emission tomography. PMd/PMv: dorsal/ventral premotor area. preSMA: presupplementary motor area. PwPD: patients with Parkinson's disease. R1: longitudinal relaxation rate. R2*: effective transverse relaxation rate. ROIs: region of interest. S1: primary somatosensory area. SMA: supplementary motor area.

Supplementary Files

This is a list of supplementary files associated with this preprint. Click to download.

- Supplementarymaterial.pdf